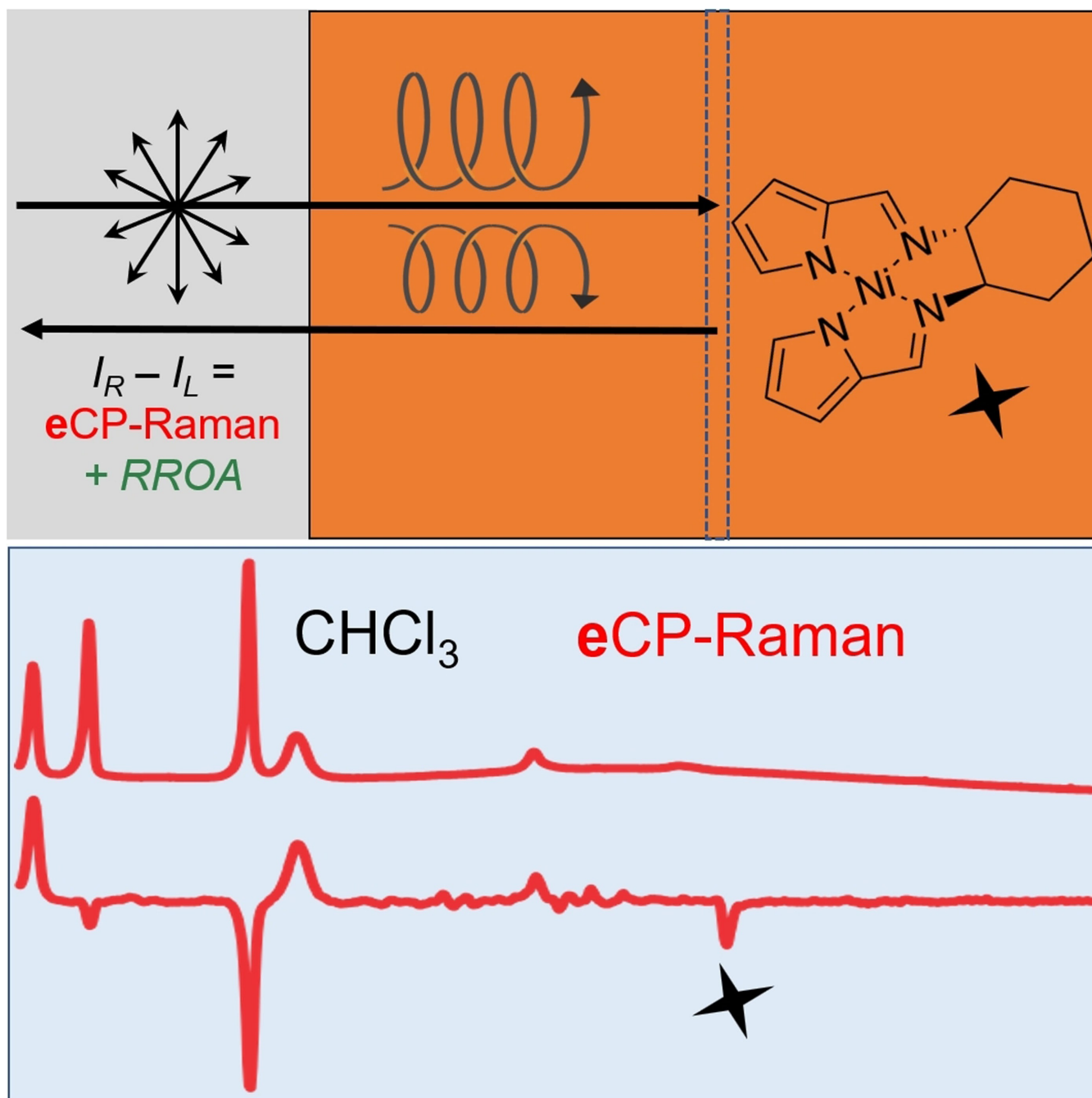


Electronic Circular Dichroism-Circularly Polarized Raman (eCP-Raman): A New Form of Chiral Raman Spectroscopy

Guojie Li,^[a] Mutasem Alshalalfeh,^[a] Josef Kapitán,^[b] Petr Bouř,^[c] and Yunjie Xu^{*[a]}



Abstract: This Concept article summarizes recent work on the development of a new form of chiral Raman spectroscopy, eCP-Raman, which combines two spectroscopies: electronic circular dichroism (ECD) and circularly polarized Raman (CP-Raman). First, some puzzling observations while carrying out Raman optical activity (ROA) measurements of several transition metal complexes under resonance are described, as well as the search for the mechanisms responsible. Then an

equation for quantifying the eCP-Raman contribution is presented, followed by several examples of how eCP-Raman influences the I_R-I_L spectra of achiral and chiral solvent molecules and of a number of chiral solutes under resonance. The conditions to extract resonance ROA, when the eCP-Raman contribution is minimized, are also discussed. Finally, we comment on the potential applications of eCP-Raman.

Introduction

First discovered in 1848 by Louis Paster,^[1] molecular chirality has continued to fascinate researchers in a wide range of fields from physics to chemistry to biology. A recent encouragement for this research direction is the 2021 Nobel Prize in Chemistry, awarded to List and MacMillan for the development of a third type of catalysis, called *asymmetric organocatalysis*.^[2] Exploration of properties of chiral molecules, such as their absolute configuration, conformations,^[3] and chirality transfer effect,^[4] has intertwined with substantial efforts in development of chiroptical spectroscopic techniques. These include, for example, electronic circular dichroism (ECD),^[5] vibrational circular dichroism (VCD)^[6] and the chiral version of Raman scattering, Raman Optical Activity (ROA).^[6a,7,8] ROA measures the small intensity difference of scattered right circularly polarized light (RCPL) versus left circularly polarized light (LCPL) and has evolved into a powerful chiroptical spectroscopic tool for characterizing chemical and biological systems.^[9] One known experimental limitation is related to the weakness of Raman signals. Since the intensity ratio of ROA over its parent Raman, i.e. normalized circular intensity difference (CID), is typically in the order of 10^{-3} to 10^{-5} ,^[6a,7] ROA measurements are quite challenging. In the mid-1970s, weeks of measuring time were needed for recording a single ROA spectrum.^[10] Different designs of instruments have been reported with considerable improvements over the years, for example, the incident circular polarization (ICP) ROA instrument in right-angle scattering^[11] and later the scattered circularly polarized (SCP)-ROA in back scattering.^[12a] In 2003, Hug created virtual enantiomers by purely optical means, combined this approach with his SCP-

ROA instrument, and demonstrated nearly artifact free ROA spectra.^[12b] Nowadays, almost all active ROA research laboratories worldwide utilize ROA spectrometers with Hug's original design.

In addition to the technical advances in ROA instruments, researchers also pursue enhancement on the molecular level. It is known that the resonance regime, i.e. when the laser excitation frequency matches one or several electronic transition(s) of the targeted molecules, provides drastic enhancement of Raman signal.^[13] Inspired by such advances, chiroptical researchers began to explore resonance ROA (RROA) both experimentally and theoretically for signal enhancement and for fundamental understanding. In 1996, Nafie proposed the single electronic state (SES) theory^[14] for RROA when only one SES is in resonance with the excitation laser wavelength, formally establishing the linkage between ECD and ROA. Based on the SES theory, all RROA bands are mono-signate, with a sign opposite to that of ECD of the resonance electronic state. This is commonly regarded as the hallmark of a RROA spectrum. In contrast, multi-signate spectra are common for off-resonance ROA measurements. Experimentally, RROA enhancements have been reported for naproxen, its derivatives,^[15] transition metal complexes,^[16] and more recently for systems such as aggregated carotenoids,^[17] and human serum transferrin.^[18] In part because of its beautiful simplicity, the SES theory has been widely utilized by experimentalists including ourselves to interpret experimental ROA results when (near) resonance is present.

Although not the focus of the current paper, we would like to point out some recent theoretical developments in treating RROA. For example, by considering excited state interference and Herzberg–Teller effects, Vidal et al. showed that a multi-signate RROA spectrum showing intensity enhancement can be produced.^[19] Other approaches, such as using the time-dependent (TD) formulation and real time propagation DFT^[20] and the finite lifetime^[21] methods have also been developed. In some cases, DFT simulated RROA spectra of systems, such as naproxen sodium, quinidine and 2-Br-hexahelicen, have been compared to the experimental data.^[20c,22]

Some intriguing chiral resonance Raman (RRaman) experimental data, especially those with huge I_R-I_L solvent bands have appeared in the last few years. These observations could not be justified by the existing theory, in spite of the significant theoretical advances in RROA. Consequently, different models were proposed and developed to explain the observations with

[a] G. Li, M. Alshalalfeh, Prof. Y. Xu
Department of Chemistry
University of Alberta, Edmonton
T6G 2G2 Alberta (Canada)
E-mail: yunjie.xu@ualberta.ca

[b] Dr. J. Kapitán
Department of Optics
Palacký University Olomouc
17. listopadu 12, 77146 Olomouc (Czech Republic)

[c] Prof. P. Bouř
Institute of Organic Chemistry and Biochemistry
Flemingovo náměstí 2, 16610 Prague (Czech Republic)

 Selected by the Editorial Office for our Showcase of outstanding Review-type articles (www.chemeurj.org/showcase).

different degrees of success. In this concept article, we focus on one important question: are the I_R-I_L signals observed under (near) resonance using a SCP-ROA spectrometer, which have been commonly regarded as RROA before, actually RROA? The answer is often not, and we aim to provide an overview of a new form of chiral Raman spectroscopy under resonance. We will start by presenting a persistent puzzle with the unexpected huge I_R-I_L solvent bands detected with a SCP-ROA spectrometer when a chiral solute is under resonance and showing the path to the discovery of this new form of chiral Raman spectroscopy. Then, we will describe the development of an equation to quantify its contribution, use several recent published examples to illustrate its effect on I_R-I_L measurements, and finally provide an outlook of its further development and its potential applications.

A few different phases have been used to describe this new form of chiral Raman spectroscopy, for example, 'two spectroscopies in one: interference of CD and ROA',^[23] *eCP-Raman*, a combination of electronic circular dichroism and circularly

polarized Raman,^[24] false ROA and ECD/ROA interference,^[25] and ECD-Raman.^[26] We will adopt the usage of a combination of ECD and circularly polarized-Raman (CP-Raman)^[7] and abbreviate it as *eCP-Raman* to emphasize the contribution of both ECD and CP-Raman in this mechanism. Furthermore, we will use I_R-I_L to label a spectrum observed in the usual channel used for regular ROA measurements using a SCP-ROA instrument, because there are multiple contributions to the I_R-I_L signal. We will also avoid using false ROA or ROA_{ECD} to describe the *eCP-Raman* contribution.

In Scheme 1, we list four molecules, *R-Ni*, *R-Cu*, *S-BN*, and B_{12} which are used as examples in the following. Their UV-Vis absorption spectra are summarized in Figure 1.

Some puzzling observations for systems under resonance

In 2014, while working on a series of transition metal complexes with the Schiff-base ligand (*R,R*) and (*S,S*)-bis(pyrrrol-2-ylmeth-

Guojie Li is currently a Ph.D. student at Department of Chemistry, University of Alberta, Canada under supervision of Prof. Xu. His research interests mainly focus on Resonance Raman Optical Activity (RROA) and more generally chiral Raman scattering events under resonance condition.



Mutasem Alshalalfeh completed his BSc in Chemistry at Birzeit University (Palestine) in 2013 and his MSc in chemistry in 2014 at the KFUPM (Saudi Arabia). Currently, he is pursuing his Ph.D. at the University of Alberta, under the supervision of Prof. Xu. His research interests mostly focus on chirality recognition and chiroptical spectroscopy of chiral molecules under resonance in Raman scattering studies.



Josef Kapitán received his PhD in Biophysics, Chemical and Macromolecular Physics from the Charles University in Prague in 2006. He then joined the group of Prof. Laurence D. Barron and Dr. Lutz Hecht at the University of Glasgow, where he developed the ROA spectrometer for the ultraviolet spectral range. Since 2010, he has been an academic senior researcher at the Palacky University Olomouc, where he specializes in research on instrumentation for spectropolarimetry, Raman and ROA spectroscopy and vibrational optical activity simulations.

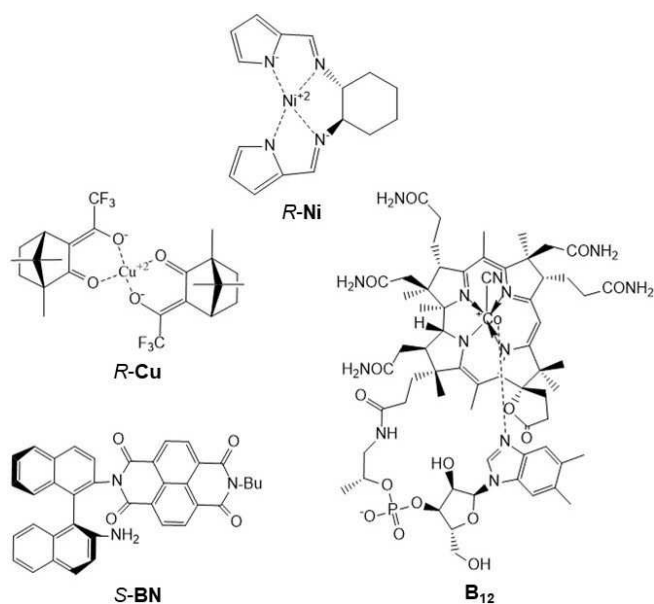


Petr Bouř received PhD in physical organic chemistry in 1993, from the Czechoslovak Academy of Sciences, in a joint program with University of Illinois at Chicago. Currently he is a professor at the University of Technology, Prague, and a Group leader at the Institute of Organic Chemistry and Biochemistry, Czech Academy of Sciences. He specializes in development of computational methods for molecular properties, theoretical and experimental aspects of chirality and vibrational optical activity.



Yunjie Xu received her PhD degree in molecular spectroscopy from the University of British Columbia, Canada in 1993 and is currently a professor and Tier I Canada Research Chair in Chirality and Chirality Recognition in the Chemistry Department at the University of Alberta. Her research focuses on exploring mechanisms of chirality recognition/transfer/amplification at the molecular level by applying and developing new spectroscopic tools to characterize structural and dynamical properties of chiral molecules and non-covalent interactions among them in the gas phase, solution, cold rare gas matrices and at liquid-liquid interfaces.





Scheme 1. The four chiral compounds discussed: (*R,R*)-bis (pyrrol-2-ylmethylethylamine)-cyclohexane nickel^{II} (*R-Ni*), *R*-bis-(trifluoroacetyl camphorato) copper^{II} (*R-Cu*), atropisomeric naphthalenediimide derivative, *S*-nBu-NDI-BINAM (*S-BN*), which consists of binaphthalenylamine (BINAM) and naphthalene (NDI), and a derivative of vitamin B₁₂, (CN)13-*epi*-Cbl(e-lactone) (**B₁₂**).

yleneamine)-cyclohexane,^[28] we observed a greatly enhanced intensity for the I_R-I_L spectra with Ni and Cu (Scheme 1). The I_R-I_L signals appeared in a few minutes rather than a few hours as typically expected. The elevated Raman baselines indicated that Ni and Cu were under (or near) resonance, leading to the initial speculation that these are RROA features. However, subsequent experiments with a range of solvents indicate that

these strong I_R-I_L bands actually belong to the achiral solvents which are *not* under resonance.

Specific non-covalent intermolecular interactions, for example hydrogen-bonding, between a chiral solute and solvent molecules, have been reported to produce the induced (chirality transferred) solvent VCD bands.^[29] However, extensive modeling of the specific Ni...solvent adducts showed no sign of any enhancement or any ROA patterns which remotely resemble the experimental observation. In 2016, an observation of intense induced I_R-I_L bands of the nitrile solvents by a helquat dye was reported and the authors suggested that some chiral arrangements of solvent molecules trapped near dihedral planes of helquat may be responsible.^[30] Could a similar mechanism be responsible in the case of Ni and Cu? After sampling several hundreds of possible structures, this idea was abandoned because Ni has a nearly planar geometry and it would be difficult to exert any chiral spatial requirement on the solvent molecules nearby.

An intriguing report of a through-space transfer of chiral information mediated by a plasmonic nanomaterial^[31] inspired some of us to search for a different mechanism. A proposal, that the observations were related to a similar through-space solvent-solute interactions, facilitated by the solute under resonance, was put forward. The transition polarizability model^[32] was then used to account for how Ni which has some large polarizabilities, affects the properties of the solvent molecules at a distance, without specific chemical binding or non-covalent interactions. Somewhat surprisingly, the model captured the observed solvent I_R-I_L pattern, i.e. relative band intensities and signs, very well,^[33] even though the predicted CID, defined as $(I_R-I_L)/(I_R+I_L)$, was too small compared to the experimental one. In addition, the model indicated that the electric-dipole/electric quadrupole Rayleigh polarizability (*A*) is primarily responsible for the induced ROA event whereas the

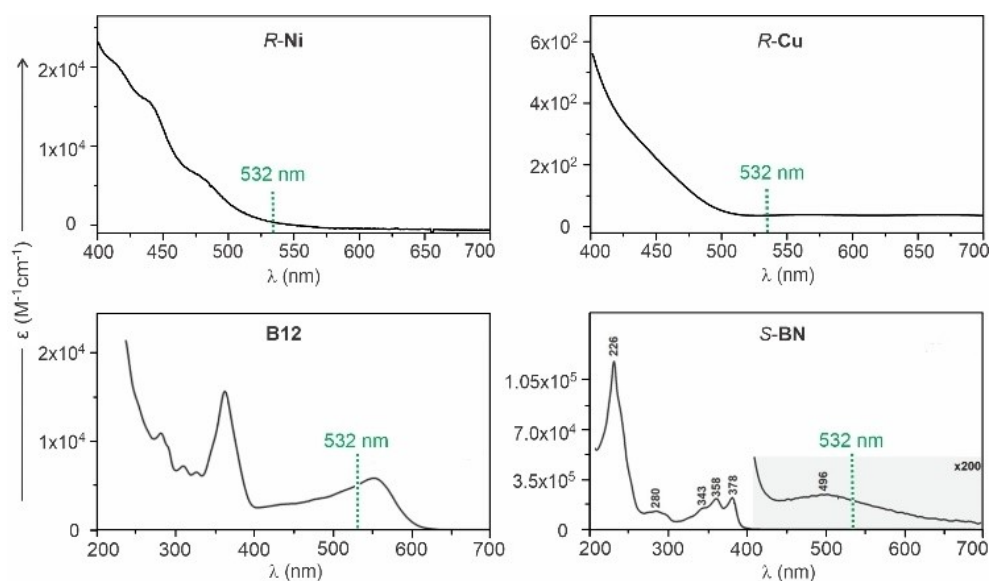


Figure 1. Experimental UV-Vis absorption spectra of the four chiral molecules in Scheme 1. The 532 nm excitation wavelength is indicated by the green dotted lines. The **B₁₂** and **S-BN** data plots are reproduced from refs. [25] and [27], respectively.

contribution of the G' tensor is negligible, in contrast to the normal ROA bands where the contribution of the G' tensor usually dominates. This led to the idea that chiral Rayleigh scattering by Ni is responsible for the intense, induced solvent I_R-I_L bands.

For the next test example, **Cu**, the same strategy failed to reproduce the experimental solvent I_R-I_L pattern, suggesting that the proposed Rayleigh mechanism may be incorrect.

More recently, a mono-signate I_R-I_L spectrum was reported for **BN**.^[27] One common characteristic with the above example is that the mono-signate solvent I_R-I_L bands are about ten times stronger than the main **BN** bands. Furthermore, it was perplexing that the experimental RROA sign of **BN** is the same as the ECD of the corresponding (near) resonance electronic transition, contrary to the SES prediction. In order to explain this observation, the authors proposed two **BN** conformers with opposite ECD signs and (near) resonance electronic transitions. While one dominates the ground state, the other overtakes the excited state. Although the authors were able to invoke the SES theory to explain the unexpected I_R-I_L sign of **BN**, the very strong solvent I_R-I_L bands could not be accounted for.

All these experimental evidences appear to point to a new mechanism which was not known at the time.

The discovery of eCP-Raman spectroscopy

The experience above indicates that it is necessary to examine all the potential light-matter interaction events during an I_R-I_L measurement when a chiral solute is under resonance. Besides the anticipated Raman and Rayleigh scatterings and their respective chiral forms, UV-vis absorption and ECD also take place at the same time in the same solution. The latter events can also contribute to the I_R-I_L signal detected as explained below.

Nowadays, almost all I_R-I_L Raman measurements are conducted using the SCP configuration where incident light is randomly polarized and the intensity differences between the scattered RCPL versus LCPL, i.e. I_R-I_L , is detected in the backscattering fashion.^[12] This scheme is illustrated in Figure 2. In these experiments, the incoming light is typically focused at the center of an optical cell and the scattered light is collected at the backward (180 degree) direction and collimated with the same focusing lens.

In a regular ROA experiment when a chiral solute is far-from resonance, the in-coming light remains randomly polarized as it travels to the laser focus point where the vast majority of Raman scattering events happen, leading to the usual ROA signal (Figure 2a). In a resonance experiment with a chiral solute, the RCPL and LCPL components of the in-coming randomly polarized light are absorbed differently, as governed by the ECD process of the chiral solute solution. Consequently, significant imbalance in RCPL versus LCPL is created as light passes through the cell. As a result, the in-coming light becomes partially circularly polarized when it reaches the laser focus point in the cell and interacts with the molecules there which undergo CP-Raman scattering (Figure 2b). The back-

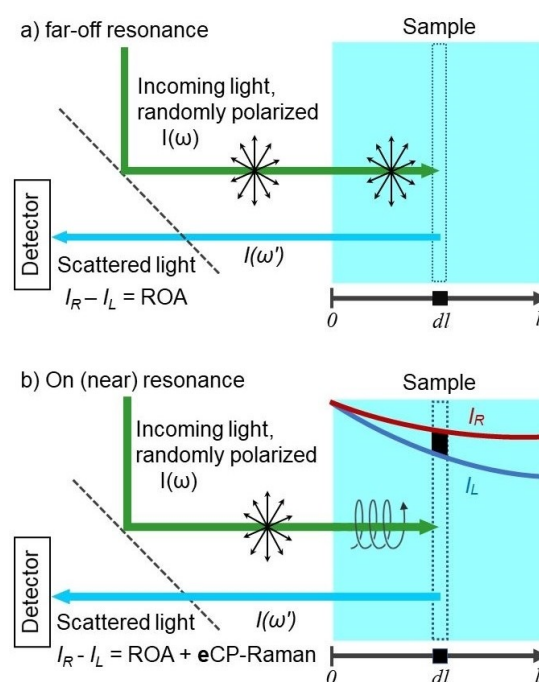


Figure 2. Geometry of a backscattering SCP-ROA experimental set up. The incoming randomly polarized light of frequency ω is typically focused at the center of the optical cell. The scattered light of frequency ω' is collected and analyzed in terms of I_R+I_L and I_R-I_L . **a)** A usual SCP-ROA experiment when the chiral solute is far-from resonance. **b)** When the chiral solute is under (near) resonance, it can absorb RCPL and LCPL differently, corresponding to its ECD. An imbalance between RCPL and LCPL is created when light arrives at the focus point where Raman scattering happens. Here the I_R-I_L signal of the scattered light of frequency ω' is no longer just ROA but also eCP-Raman. Please see the main text for further description. Note that the spiral in **b)** simply indicates the imbalance after light enters the solution and its intensity does not reflect how the intensity changes along the path. Also, I_R and I_L would eventually decay to zero if the absorption is very strong, although that is not the typically experimental condition used in the studies discussed here. Please refer to Figure S2 of Ref. [23] for further discussion.

scattered light experiences further ECD absorption as it passes through the solution to the detector, leading to the final eCP-Raman signal. We note that the usual Raman and the associated RROA events also happen as expected, and the relative magnitude of RROA with respect to eCP-Raman will be discussed later.

CP-Raman scattering was described by Placzek in 1934^[34] and may be easier to grasp by comparing it to linearly polarized Raman scattering. CP-Raman scattering measurements are typically carried out by using 100% RCPL (or LCPL) for excitation and monitoring the I_R-I_L (or I_L-I_R) signals in scattering. The *DOC* value, the normalized degree of circularity, is defined as the ratio of the intensity difference of the circularly polarized components to the total intensity. In a CP-Raman experiment, this can be written as $DOC = (I_R - I_L) / (I_R + I_L)$ when one uses 100% excitation RCPL. We treat *DOC* as a molecular property and follow the convention used in Ref. [6a] where the intensity difference in the numerator is always co-rotating minus contra-rotating intensity and the ratio has a sign depending on whether the co-rotating or contra-rotating scattering is more intense. Quantum mechanically, the intensity and sign of

CP-Raman signals are calculated using the same electric dipole-electric dipole polarizability tensors as for Raman scattering. The *DOC* value varies from +5/7 for depolarized bands to −1 for completely polarized bands under the far-from resonance conditions.^[6a]

The utility of CP-Raman was explored mainly in the 70s and 80s^[35] and some related work continues.^[36] These CP-Raman experiments were often carried out using the Raman backscattering configuration.^[35a,36] It is important to emphasize that CP-Raman I_R-I_L signals can be observed for chiral or achiral molecules and their intensity is similar to that of Raman, generally much larger compared to that of ROA. For example, multi-signate CP-Raman spectra of achiral solvents such as chloroform and benzene or of chiral ferrocyclochrome c can be found in the papers by Clark et al.^[35a] or by Nestor et al.,^[35b] respectively.

In summary, under resonance, I_R-I_L contains two contributions, i.e. RROA and eCP-Raman. For the eCP-Raman contribution, the following expression was derived^[23]

$$CID = \frac{I_R - I_L}{I_R + I_L} = \frac{\ln 10}{4} cL \Delta \varepsilon \left(\frac{\Delta \varepsilon'}{\Delta \varepsilon} + DOC \right) \quad (1)$$

Here, $\Delta \varepsilon$ and $\Delta \varepsilon'$ are decadic, differential absorption coefficients of the chiral solute for the excitation light at 532 nm and for the scattered light at each Raman band, respectively. c is the concentration of the chiral solute, L is the optical path length, *DOC* is the normalized degree of circularity of the vibrational transition of interest, and I_R and I_L are the intensities of scattered RCPL and LCPL registered at the ROA instrument, respectively. The factor $\ln 10$ is added since decadic absorption coefficients are used.^[24,25] A step-by-step derivation of equation (1) was provided in Ref. [23] and a brief summary is given below.

First, the differential absorption of the incident light I_0 at 532 nm is $\Delta \varepsilon = \varepsilon_L - \varepsilon_R$ where ε_L and ε_R are the molar absorption coefficients of LCPL and RCPL, respectively. After the in-coming light travels a distance of l , the intensities of RCPL and LCPL can be expressed as

$$\begin{aligned} I^R(l) &= I_0 e^{-\varepsilon_R c l} / 2 \\ I^L(l) &= I_0 e^{-\varepsilon_L c l} / 2 \end{aligned} \quad (2)$$

In the detected intensities, we use the superscripts for excitation light and the subscripts for scattered light. In a backscattering I_R-I_L measurement, each finite volume element dl contributes to the scattered intensities as

$$\begin{aligned} dI_L^s &= a I^L(l) dl + b I^R(l) dl \\ dI_R^s &= a I^R(l) dl + b I^L(l) dl \end{aligned} \quad (3)$$

Here, a and b are the depolarization coefficients which depend on transition polarizabilities of the solvent. Therefore, the total Raman intensity is as

$$dI_{Raman}^s(l) = dI_R^s + dI_L^s = (a+b)(I^R(l) + I^L(l)) dl \quad (4)$$

Second, consider the absorption of the outgoing Raman scattering light by the chiral solute solution under resonance by using the Lambert-Beer law, we get at $l=0$

$$dI_{Raman}^s(0) = (a+b)[I^R(l)e^{-\varepsilon_R' c l} + I^L(l)e^{-\varepsilon_L' c l}] dl \quad (5)$$

With a negligible error, we can assume that $\varepsilon_L \approx \varepsilon_R \approx \varepsilon$ (at 532 nm) and $\varepsilon_L' \approx \varepsilon_R' \approx \varepsilon'$ (at other wavelengths) and combine equation (5) with (2) to arrive at equation (6)

$$dI_{Raman}^s(0) = (a+b)I_0 e^{-(\varepsilon'+\varepsilon)c l} dl \quad (6)$$

A similar strategy could be used to derive the I_R-I_L signal, i.e. the intensity difference (eCP-Raman) detected by a commonly used SCP chiral Raman instrument

$$\begin{aligned} dI_{eCP-Raman}^s(0) &= [a I^R(l) dl + b I^L(l) dl] e^{-\varepsilon_R' c l} \\ &\quad - [a I^L(l) dl + b I^R(l) dl] e^{-\varepsilon_L' c l} \\ &= \left(a + b e^{-\Delta \varepsilon c l} - a e^{-(\Delta \varepsilon + \Delta \varepsilon') c l} - b e^{-\Delta \varepsilon' c l} \right) \\ &\quad I_0 e^{-(\varepsilon'+\varepsilon)c l} dl / 2 \end{aligned} \quad (7)$$

By carrying out the necessary integration, the CID defined as $(I_R-I_L)/(I_R+I_L) = (I_R-I_L)/I_{Raman}$ for weak absorption where $cL(\varepsilon'+\varepsilon) \ll 1$, becomes

$$CID \cong \frac{a(\Delta \varepsilon + \Delta \varepsilon') + b(\Delta \varepsilon' - \Delta \varepsilon) cL}{a+b} \frac{cL}{4} \quad (8)$$

The depolarization coefficients a and b are related to the *DOC* of a Raman transition of the achiral solvent^[6a] by

$$DOC = \frac{a-b}{a+b} \quad (9)$$

Rearranging equation (8) and substituting (9) into (8) finally leads us to equation (1) which quantifies the eCP-Raman contribution. We note that equation (1) was derived for uniform scattering and ECD absorption along the laser beam, whereas in reality, scattering is limited to a smaller volume as illustrated in Figure 2. A slight modification of equation (1) was proposed to account for the difference in the ECD versus Raman/ROA active path.^[25] With this tool in hand, it is now possible to simulate eCP-Raman spectra of solvents which are not under resonance themselves.

The I_R-I_L spectra of solvent molecules with a chiral solute under resonance

Armed with equation (1) for the eCP-Raman contribution, we examine the I_R-I_L spectra of CHCl_3 with **Ni** and **Cu**. In Figure 3, the experimental ECD spectra of **Ni** and **Cu** and their corresponding I_R-I_L spectra in CHCl_3 are presented. All visible I_R-I_L spectral bands are associated with the CHCl_3 Raman bands

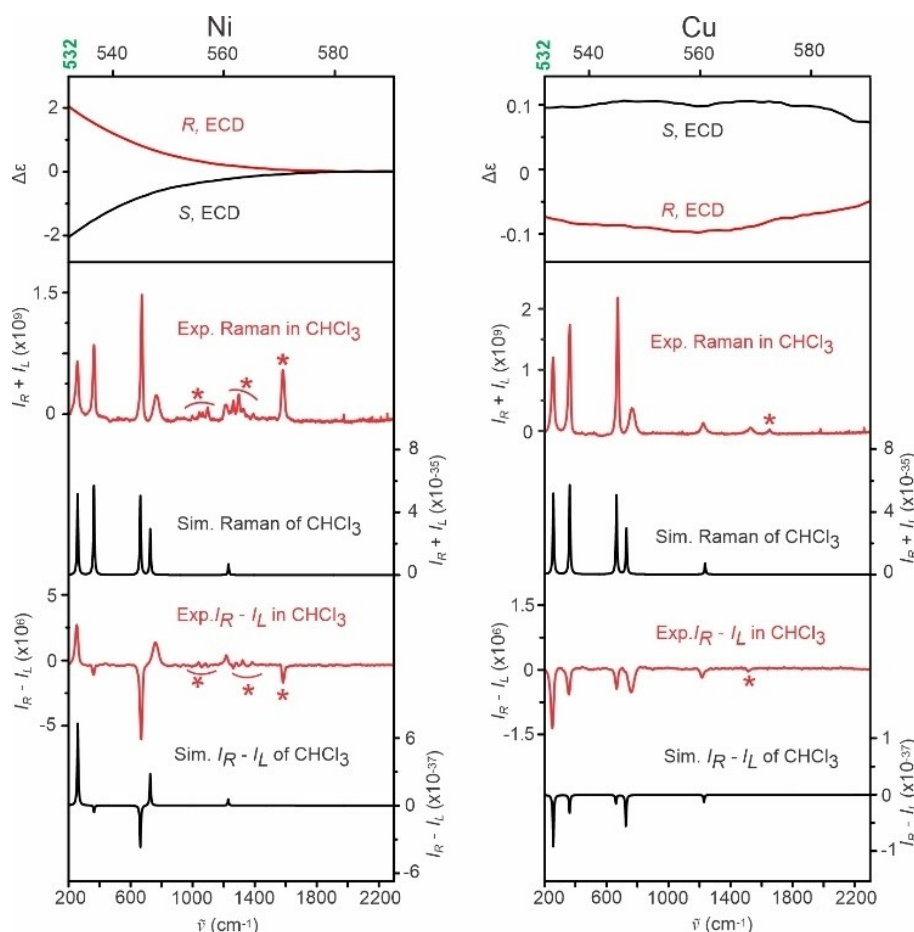


Figure 3. Top: Experimental ECD spectra ($\Delta\epsilon$, $\text{Lmol}^{-1} \text{cm}^{-1}$) of **Ni** and **Cu**. Bottom: The experimental (red) $I_R + I_L$ (Raman) and $I_R - I_L$ spectra of **R-Ni** (left) and **R-Cu** (right) in CHCl_3 and the simulated $I_R + I_L$ (Raman) of pure CHCl_3 and simulated $I_R - I_L$ spectra of CHCl_3 with **R-Ni** (left) and with **R-Cu** (right). The simulated $I_R - I_L$ (eCP-Raman) are computed as Raman \times CID where the CID curve was calculated based on equation (1) using the experimental $\Delta\epsilon$ and $\Delta\epsilon'$ values and the simulated DOC curve. The simulated $I_R + I_L$ and $I_R - I_L$ are in $\text{m}^2 \text{cm}/\text{sr}$ and are scaled with the respective solvent or solute concentration and path length. * indicates bands assigned to **R-Ni** or **R-Cu**. The figures are produced based on the data reported in Ref. [23] and [33].

except those fairly weak bands marked with * which are assigned to the solute bands of **Ni** or **Cu**, vide infra. To simulate the eCP-Raman spectra of CHCl_3 with **Ni** and with **Cu**, the experimental ECD spectra were used directly, together with the experimental values of $[\text{Ni}]$, $[\text{Cu}]$ and L used in the Raman scattering experiments. The Raman spectrum of CHCl_3 and its DOC values were calculated at the B3LYP/CC-PVTZ level using the Gaussian program.^[37] The DOC values can also be obtained experimentally using a BioTools SCP-ROA spectrometer by placing a quarter waveplate into the incoming laser beam path to make it circularly polarized.^[26,36]

As one can see, the experimental $I_R - I_L$ spectral features of CHCl_3 with **Ni** and with **Cu** are well reproduced by the simulated $I_R - I_L$ spectra. Not only the relative intensities and signs of the solvent bands, but also the experimental CID values of these solvent bands in the order of 10^{-3} for **Ni** and 10^{-4} for **Cu** are captured by the simulations. Essentially, the $I_R - I_L$ spectral features of CHCl_3 provide information about chirality of **Ni** or **Cu** through the eCP-Raman mechanism. In some publications, such features are also labeled as markers of *chirality transfer* where

chirality of a chiral molecule is sensed by an achiral molecule. Since the process (or mechanism) is through space, without any chemical or non-covalent intermolecular interactions between the two parties, some researchers prefer not to refer to this as chirality transfer. We note that the term *chirality transfer* was also used before where the transfer was facilitated by plasmons through space.^[31]

Since these chiral transition metal complexes, such as the **Ni** complex, tend to have an extremely large magnetic dipole moments associated with the d-d electronic transitions and their dissymmetry factors, g , i.e. the ratio of intensity of ECD over that of UV-vis absorption, are generally pretty large. This factor, together with the large Raman intensity of CHCl_3 , gives rise to the very strong solvent $I_R - I_L$ features, often overwhelming the $I_R - I_L$ features of the solute itself, as in the **Ni** and **Cu** examples. While specific non-covalent interactions and coordination may still produce induced solvent chirality features, it is important to check if the eCP-Raman mechanism plays an important role in solvent $I_R - I_L$ signals for resonance measurements.

An interesting and special case is the I_R-I_L measurement of 2-butanol, a chiral solvent, with Ni^[33] which is under (near) resonance, whereas 2-butanol is far-from resonance. The natural ROA spectrum of 2-butanol neat liquid has a CID value in the order of $10^{-4} \sim 10^{-5}$, considerably smaller than the CID generated by the eCP-Raman mechanism for the Ni system, of the order of 10^{-3} . In Figure 4, the experimental I_R-I_L features of 2-butanol with Ni (Figure 4b) are compared to those of the natural ROA features of *R*-2-butanol (Figure 4c), showing completely different patterns from each other. What are these the experimental I_R-I_L features? Since the *R*-2-butanol:CDCl₃ (2:3) mixture contain complex hydrogen-bonding interactions, it would be difficult to model its Raman and CP-Raman well, we chose to extract an experimental DOC curve by using the ratio of the experimental CP-Raman and Raman spectra of the same mixture. The *R*-Ni ECD and experimental DOC values are used in equation (1), together with the experimental Ni concentration and optical path to simulate the corresponding eCP-Raman spectrum of the solvent mixture.

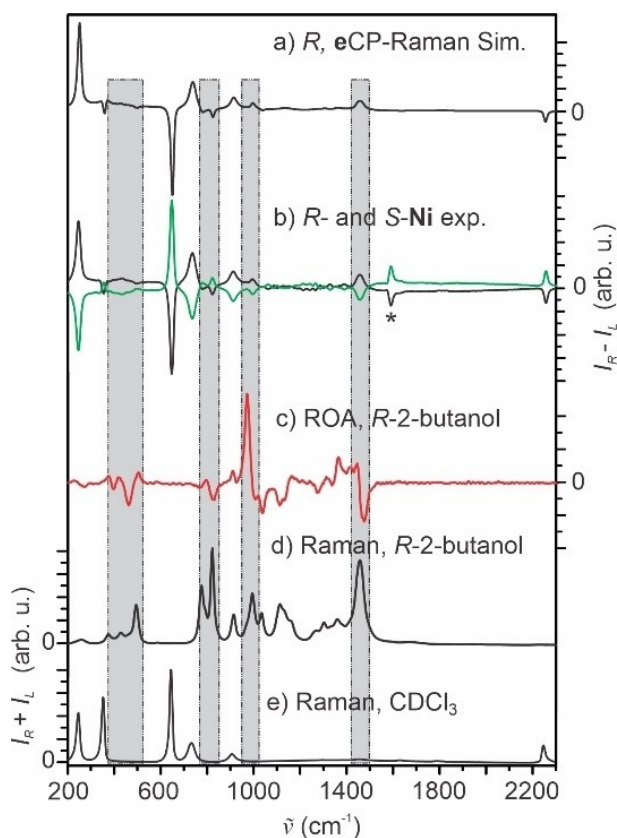


Figure 4. a) Simulated eCP-Raman spectrum of a mixture of *R*-2-butanol:CDCl₃ (2:3) based on the experimental CP-Raman and Raman spectra of the same mixture and *R*-Ni ECD using equation (1). See the main text for detail. b) The experimental I_R-I_L signals of *R*-Ni (black) and *S*-Ni (green) in a mixture of *R*-2-butanol:CDCl₃ (2:3) solvent. Experimental c) ROA and d) Raman spectra of neat liquid *R*-2-butanol. e) Experimental Raman spectrum of pure CDCl₃. The strongest Ni bands at 1588 cm⁻¹ are marked by an asterisk *. The four rectangular boxes highlight the 2-*R*-butanol ROA bands in c) which show no resemblance to the corresponding I_R-I_L signals in b). The latter was well reproduced by the simulated eCP-Raman in a). The figure is produced based on the data reported in Ref. [33].

In Figure 4b, the experimental I_R-I_L features of *R*-2-butanol with *R*-Ni versus *S*-Ni show good mirror-images to each other, indicating that the chiral responses of *R*-2-butanol observed are dictated by the chirality of Ni, rather than the natural chirality of *R*-2-butanol. Clearly, one can see that the experimental I_R-I_L features of *R*-2-butanol with *R*-Ni (Figure 4b, black trace) are well reproduced by the corresponding eCP-Raman simulation with *R*-Ni (Figure 4a). So are the related features of CDCl₃. The 2-butanol example demonstrates that the eCP-Raman effect can totally overwrite the natural ROA response of a chiral molecule which is not under-resonance. How about the relative contributions of eCP-Raman versus the natural RROA of the chiral solute itself which is under resonance? This question will be addressed in the next section.

The I_R-I_L spectral features of a chiral solute under resonance

The success of the eCP-Raman mechanism with the far-from resonance (chiral) solvent molecules led several groups to take on the challenge of analyzing the I_R-I_L measurement of a chiral solute under resonance. Naturally one can expect contributions from both the eCP-Raman and RROA mechanisms although their relative importance was never explored before. Below we will use the I_R-I_L spectra of Ni, Cu, BN and B₁₂ as examples to discuss several interesting aspects.

In Figure 5, the experimental Raman and I_R-I_L spectra of Ni and Cu in two different solvents, dichloromethane (DCM) and chloroform (CHCl₃) are depicted. The experimental Raman and the corresponding I_R-I_L bands of Ni and Cu are numbered, while the solvent bands are indicated with asterisk. The simulated Raman spectra of Ni and Cu show a good agreement to the experimental ones, whereas the simulated RROA spectra differ noticeably from the experimental I_R-I_L spectral features. On the other hand, the simulated eCP-Raman spectra based on equation (1) can capture all the I_R-I_L spectral features including signs and relative intensities. Importantly, the magnitude of predicted CID is in the order of 10^{-3} for Ni and 10^{-4} for Cu, agreeing well with the respective experimental values. Indeed, experimentally, a few hundred scans which take less than 10 mins are sufficient to obtain a good quality I_R-I_L spectrum for Ni, whereas for Cu, a few thousand scans are needed. Overall, the dominant contributions to the I_R-I_L spectra of these two metal complexes are from the eCP-Raman mechanism, while the RROA intensities are predicted to be about 5 to 6 times weaker.

For the simulated spectra of Ni and Cu shown in Figure 5, the finite-lifetime (or damped response) approach^[38] was applied to treat the resonance effect properly, using the Gaussian Development Version (GDV) package.^[39] While the simulation of CP-Raman requires only the same polarizability tensors (electric dipole – electric dipole, α) as for Raman, the additional electric dipole – magnetic dipole and electric dipole – electric quadrupole polarizabilities (G' and A , respectively) are needed for ROA.^[7] In the current GDV version, a fully analytic derivative implementation was used for differentiating the α , G' and A polarizability tensors with respect to nuclear coordinates.

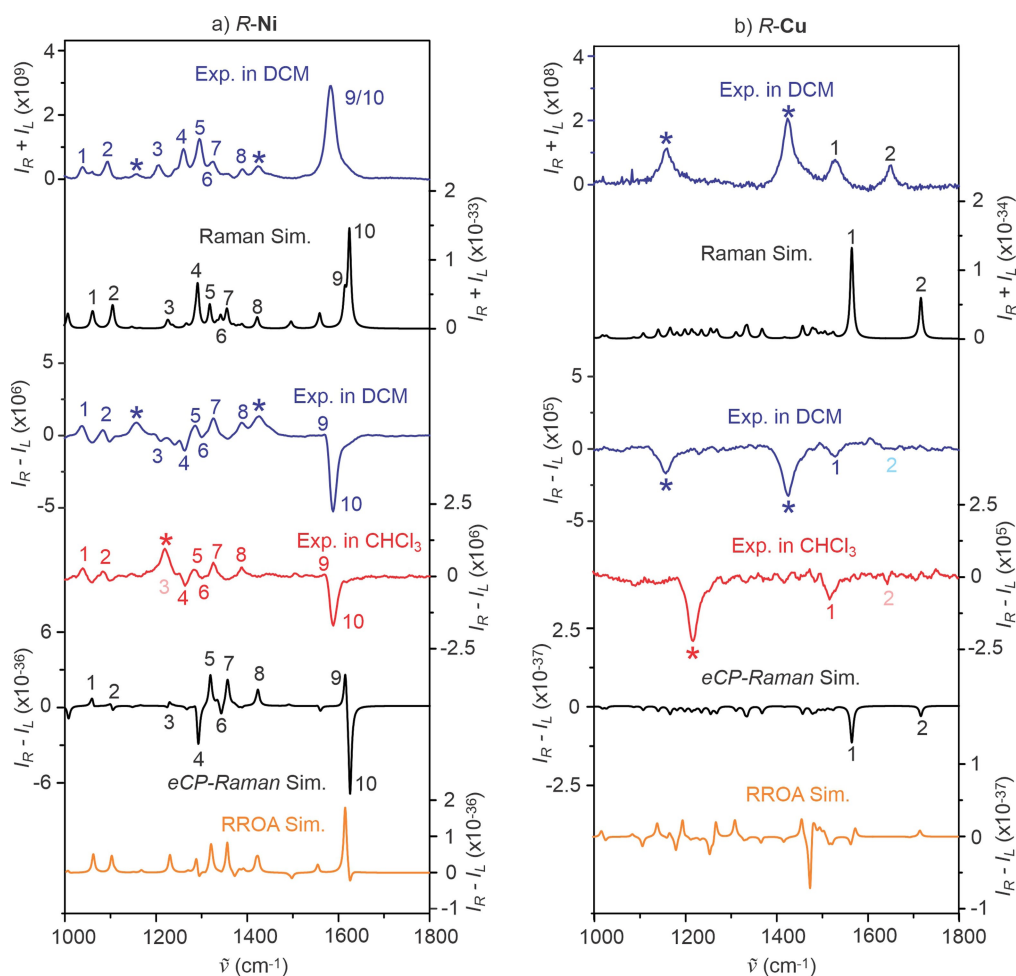


Figure 5. a) Top: experimental Raman ($I_R + I_L$) spectrum of *R*-Ni in CH_2Cl_2 (blue) is compared with the simulated one (black); Bottom: experimental $I_R - I_L$ spectra of *R*-Ni in CH_2Cl_2 (blue) and in CHCl_3 (red) are compared with the simulated eCP-Raman (black) and the simulated natural RROA spectrum (orange). b) Analogous results for *R*-Cu. Corresponding experimental and theoretical solute bands are numbered and asterisk (*) indicates the solvent bands. The calculated spectral intensities are displayed in units of $[\text{m}^2 \text{cm}^2/\text{sr}]$ where m is meter and sr is steradian. (Reproduced from ref. [24] with permission, Copyright 2021, Wiley).

As before, the GDV version includes gauge independent atomic orbitals (GIAOs) which ensure origin-independent result. These calculations typically take only about 1.5 to 2 times longer than a normal Raman and ROA calculation (i.e. without the finite-lifetime approach) with Gaussian16.^[37] Among the four examples discussed here, Ni appears to be the only one whose RRaman, CP-RRaman, and RROA spectra are noticeably influenced by the finite-lifetime approach.

With the proper mechanism in hand, the puzzling BN $I_R - I_L$ spectra observed can now be fully explained, as summarized in Figure 6. The $I_R - I_L$ band features of achiral solvents (CHCl_3 and CH_3CN) and of *S*-BN observed experimentally are all correctly predicted by eCP-Raman. An even more satisfying point is that the intensity ratios of the experimental $I_R - I_L$ bands of CHCl_3 and CH_3CN to the main band of *S*-BN, which is about 10, is reproduced by the simulations.

The above three examples demonstrate that the appearances of eCP-Raman spectra depend delicately on the term $(\Delta\epsilon'/\Delta\epsilon + \text{DOC})$ where DOC is from -1 to $5/7$. For example, for

Cu, the ECD value remains nearly constant over the full experimental Raman wavenumber scale, therefore $\Delta\epsilon'/\Delta\epsilon$ is nearly 1 and the $(\Delta\epsilon'/\Delta\epsilon + \text{DOC})$ term remains mono-signate. For BN, although its ECD value decays from 532 to 610 nm (corresponding to 0 to 2400 cm^{-1} on the Raman scale), the $I_R - I_L$ spectrum still appears to be largely mono-signate. Clearly, a mono-signate $I_R - I_L$ spectrum does not necessary imply that the SES mechanism is in play.

The possibility to extract RROA features was discussed by Machalska et al.^[25] working with a series of Vitamin B₁₂ derivatives. In the $I_R - I_L$ measurements of some Vitamin B₁₂ derivatives, the authors observed a pronounced dependence of the $I_R - I_L$ signs on the concentration of B₁₂. These B₁₂ derivatives have relatively large ECD absorption bands from 532 to 610 nm, corresponding to 0 to 2500 cm^{-1} in the Raman scale. Therefore, they can be regarded as (near) resonance at 532 nm.

These authors demonstrated that for (CN)13-epi-Cbi(e-lactone), B₁₂, they were able to flip the sign of its $I_R - I_L$ spectrum by increasing [B₁₂] from 0.1 mg/mL to 1.0 mg/mL. Based on

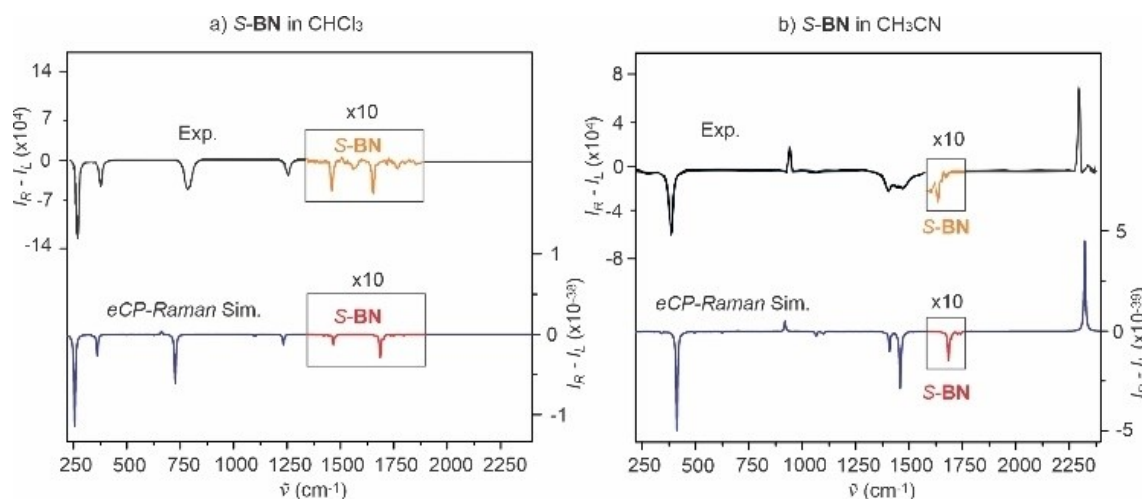


Figure 6. a) Top: the experimental $I_R - I_L$ spectra^[27] of the chiral solute *S*-BN whose bands are shown in the rectangle box and their intensities amplified by a factor of ten, and of achiral solvent CHCl_3 whose bands are those outside the box; Bottom: the corresponding simulated eCP-Raman spectra. b) Parallel plots as in a) but with *S*-BN in CH_3CN solution. (Reproduced from ref. [24] with permission, Copyright 2021, Wiley).

equation (1), the eCP-Raman spectrum can be calculated as CID times Raman where the CID magnitude is proportional to $[\text{B}_{12}]$ and the ECD path length, L , while the Raman intensity is proportional to $[\text{B}_{12}]$. Consequently, the eCP-Raman intensity depends on $[\text{B}_{12}]^2$ and the ECD path length, whereas the RROA intensity of B_{12} is just proportional to $[\text{B}_{12}]$. As a result, one can tune the relative contributions of eCP-Raman versus RROA by adjusting $[\text{B}_{12}]$ and flip the $I_R - I_L$ sign if these two contributions generate opposite signs. Similarly, by using a much shorter ECD path length, i.e. focusing the laser beam at the front of the cell instead closer to the far end of the cell, these authors were able to reduce the contribution of the eCP-Raman mechanism significantly to the extent that the RROA intensity becomes the dominant one, as shown in Figure 7.

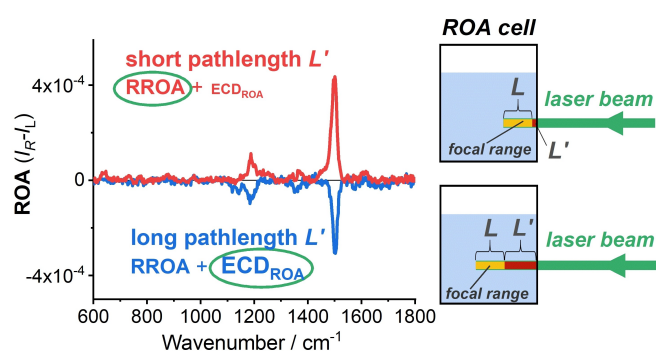


Figure 7. The experimental $I_R - I_L$ spectra of B_{12} at a concentration of 0.8 mg ml^{-1} measured for two different cell positions. Top: with the laser focus point very close to the front of the cell and therefore RROA dominates. Bottom: with the laser focus point further away from the front of the cell so that the ECD optical path is lengthened significantly and eCP-Raman dominates. (Reproduced from ref. [25] with permission, Copyright 2021, Wiley).

A recent application

Even though eCP-Raman was only very recently discovered, Kaczor and co-workers already applied this form of spectroscopy to study chirality recognition by a stereodynamic vanadium probe.^[26] Oxo-vanadium(V) aminotriphenolate, a chiral probe which was proposed as a CD stereodynamic sensor for a large variety of chiral analytes,^[40] exists as an ECD-silent racemic mixture of interconverting stereoisomers. In the presence of a chiral ligand, like *R*- or *S*-*N*-(1-phenylethyl) acetamide, the vanadium complex would form two diastereomers in different proportions because of chirality recognition interactions, giving rise to an intense ECD signal. While chiral ligand itself has weak ROA, strong induced solvent eCP-Raman signals were recorded. A noticeable advantage is that such eCP-Raman measurements could be performed at very low concentrations. For example, for *N*-(1-phenylethyl) acetamide, good spectra were obtained using only 2 micrograms of the compound, indicating that the sensitivity of the eCP-Raman method is comparable to conventional ECD spectroscopy. Since eCP-Raman bands have significantly better resolution than ECD, this may evolve into a straightforward and reliable methods for determination of enantiomeric excess of chiral samples such as new pharmaceuticals.

Summary

In this concept article, we introduce a recently developed, new form of chiral Raman spectroscopy, i.e., eCP-Raman. The mechanism for eCP-Raman is described and the derivation of the theoretical model to predict the eCP-Raman contribution is elaborated. In particular, the major differences between natural RROA and eCP-Raman in terms of their mechanisms and quantum chemistry treatments are discussed. In the $I_R - I_L$ measurements, the contaminations due to the ECD absorption

can dominate, and, in some cases, such as the examples presented, eCP-Raman can totally hide the natural RROA signals. Since this effect is common for the under (near) the resonance measurements, researchers need to consider this new mechanism when interpreting the I_R-I_L spectra. Otherwise, some misleading conclusions can be drawn. Some experimental tricks to minimize eCP-Raman are also described and the true RROA experimental data obtained are expected to play a significant role in the current development of theoretical treatments of RROA.

Generally, any color chiral compound which is under (near) resonance can invoke eCP-Raman in itself or in another Raman-scattering medium, such as a solvent, when using a common ROA instrument with visible lasers as a light source. An ROA instrument using a deep ultraviolet laser at 244 nm was reported already,^[41] offering the possibility to carry out eCP-Raman of chiral molecules which are transparent to visible light, such as peptides, proteins and nucleic acids.

We see potential applications of eCP-Raman in five different areas: 1) Extracting true RROA by removing the eCP-Raman contribution to I_R-I_L ; 2) Untangling different chirality transfer mechanisms reported using ROA measurements, for example, by separating those due to inter/intramolecular bonding interactions from those through space transfer (such as in the case of eCP-Raman); 3) Offering chirality detection and absolute configuration determination, as a new stand-alone chiral spectroscopy with a chirality sensitivity often much greater than regular ROA and comparable to ECD; 4) Offering an alternative way of measurement of ECD.^[26] Although detection of ECD through eCP-Raman does not bring particular advantages against direct ECD measurement currently, the sensitivity limit of eCP-Raman is already comparable and the related ECD can be detected easier in cases of strongly absorbing compounds; 5) Providing additional information such as polarized Raman scattering to unpolarized Raman measurement. Quite often, with eCP-Raman, the contribution of the degree of circularity of the Raman-scattering part of the sample dominates. This part corresponds to polarized Raman scattering, thus providing information about molecular polarizabilities. Since eCP-Raman is very new, one can expect its further development and exciting new applications along the way.

The experimental results and theoretical modelling presented herein demonstrate that eCP-Raman is a promising tool to study the natural chirality and structural properties in chiral systems under resonance. Importantly, eCP-Raman, as a new type of chiral Raman spectroscopy, combines the high chirality sensitivity of ECD with high resolution capability of Raman spectroscopy, thus offering experimental advantages in untangling some complex excited state phenomena.

Acknowledgements

We thank Drs. L. D. Barron, P. L. Polavarapu, J. R. Cheeseman for discussions. This work was funded by the Natural Sciences and Engineering Research Council of Canada, the Canada Foundation for Innovation, Alberta Enterprise, Advanced Education, the

University of Alberta and Compute Canada, and by the Grant Agency (22-04669S) and Ministry of Education (CZ.02.1.01/0.0/0.0/16_019/0000729) of the Czech Republic. G. L. acknowledges Alberta Excellence Graduate Scholarship and Gunning Physical Chemistry Fellowship. Y. X. is Tier I Canada Research Chair in Chirality and Chirality Recognition.

Conflict of Interest

The authors declare no conflict of interest.

Data Availability Statement

The data that support the findings of this study are available in the supplementary material of this article.

Keywords: circularly polarized Raman · electronic circular dichroism · new chiral Raman spectroscopy: eCP-Raman · resonance Raman optical activity

- [1] L. Pasteur, *Ann. Chim. Phys.* **1848**, *24*, 442–459.
- [2] <https://www.nobelprize.org/prizes/chemistry/2021/press-release/>.
- [3] a) T. Fujisawa, K. Nishikawa, J. Tamogami, M. Unno, *J. Phys. Chem. Lett.* **2021**, *12*, 9564–9568; b) T. Vermeyen, J. Brence, R. V. Echelpoel, R. Aerts, G. Acke, P. Bultinck, W. Herrebout, *Phys. Chem. Chem. Phys.* **2021**, *23*, 19781–19789; c) C. Merten, F. Li, K. Bravo-Rodriguez, E. Sanchez-Garcia, Y. Xu, W. Sander, *Phys. Chem. Chem. Phys.* **2014**, *16*, 5627–5633.
- [4] a) C. Merten, Y. Xu, *Agnew. Chem. Int. Ed.* **2013**, *125*, 2127–2130; b) G. Yang, Y. Xu, *J. Chem. Phys.* **2009**, *130*, 164506.
- [5] G. Pescitelli, L. D. Bari, N. Berova, *Chem. Soc. Rev.* **2014**, *43*, 5211–5233.
- [6] a) L. A. Nafie, in *Vibrational Optical Activity: Principles and Applications*, Wiley, Chichester, **2011**; b) G. Yang, Y. Xu, *Top. Curr. Chem.* **2011**, *298*, 189–236; c) N. Sato, *Phys. Chem. Chem. Phys.* **2020**, *22*, 7671–7679.
- [7] W. Hug, S. Kint, G. F. Bailey, J. R. Scherer, *J. Am. Chem. Soc.* **1975**, *97*, 5589–5590.
- [8] a) L. D. Barron, in *Molecular Light Scattering and Optical Activity*, Cambridge University Press, Cambridge, UK, **2004**; b) G. Zajac P. Bouř, *J. Phys. Chem. B* **2022**, *126*, 355–367.
- [9] L. D. Barron, *Biomed. Spectrosc. Imaging* **2015**, *85*, 223–253.
- [10] W. Hug, S. Kint, G. F. Bailey, J. R. Scherer, *J. Am. Chem. Soc.* **1975**, *97*, 5589–5590.
- [11] L. Hecht, L. D. Barron, *J. Raman Spectrosc.* **1994**, *25*, 443–451.
- [12] a) W. Hug, G. Hangartner, *J. Raman Spectrosc.* **1999**, *30*, 841–852; b) W. Hug, *Appl. Spectrosc.* **2003**, *57*, 1–13.
- [13] See for example: E. V. Efremov, F. Ariese, C. Gooijer, *Anal. Chim. Acta* **2008**, *606*, 119–134.
- [14] L. Nafie, *Chem. Phys.* **1996**, *205*, 309–322.
- [15] M. Vargek, T. B. Freedman, E. Lee, L. A. Nafie, *Chem. Phys. Lett.* **1998**, *287*, 259–364.
- [16] C. Merten, H. Li, L. A. Nafie, *J. Phys. Chem. A* **2012**, *116*, 7329–7336.
- [17] M. Dudek, E. Machalska, T. Oleszkiewicz, E. Grzebelus, R. Baranski, P. Szcześniak, J. Mlynarski, G. Zajac, A. Kaczor, M. Baranska, *Angew. Chem. Int. Ed.* **2019**, *58*, 8383–8388; *Angew. Chem.* **2019**, *131*, 8471–8476.
- [18] J. Bogaerts, C. Johannessen, *J. Raman Spectrosc.* **2019**, *50*, 641–646.
- [19] L. N. Vidal, T. Giovannini, C. Cappelli, *J. Phys. Chem. Lett.* **2016**, *7*, 3585–3590.
- [20] a) S. Luber, J. Neugebauer, M. Reiher, *J. Chem. Phys.* **2010**, *132*, 044113; b) A. Baiardi, J. Bloino, V. Barone, *J. Chem. Theory Comput.* **2018**, *14*, 6370–6390; c) J. Mattiat, S. Luber, *J. Chem. Phys.* **2019**, *151*, 234110.
- [21] L. Jensen, J. Autschbach, G. C. Schatz, *J. Chem. Phys.* **2005**, *122*, 224115.
- [22] a) S. Luber, M. Reiher, *ChemPhysChem* **2010**, *11*, 1876–1887; b) F. Krausbeck, J. Autschbach, M. Reiher, *J. Phys. Chem. A* **2016**, *120*, 9740–9748; c) L. Abella, H. D. Ludowieg, J. Autschbach, *Chirality* **2020**, *32*, 741–752.

- [23] T. Wu, G. Li, J. Kapitán, J. Kessler, Y. Xu, P. Bouř, *Angew. Chem. Int. Ed.* **2020**, *59*, 21895–21898; *Angew. Chem.* **2020**, *132*, 22079–22082.
- [24] G. Li, M. Alshalalfeh, Y. Yang, J. R. Cheeseman, P. Bouř, Y. Xu, *Angew. Chem. Int. Ed.* **2021**, *60*, 22004–22009.
- [25] E. Machalska, G. Zajac, A. J. Wierzba, J. Kapitán, T. Andruniów, M. Spiegel, D. Gryko, P. Bouř, M. Baranska, *Angew. Chem. Int. Ed.* **2021**, *60*, 21205–21210.
- [26] E. Machalska, N. Hachlica, G. Zajac, D. Carraro, M. Baranska, G. Licini, P. Bouř, C. Zonta, A. Kaczor, *Phys. Chem. Chem. Phys.* **2021**, *23*, 23336–23340.
- [27] E. Machalska, G. Zajac, M. Baranska, D. Kaczorek, R. Kawęcki, P. F. J. Lipiński, J. E. Rode, J. Dobrowolski, *Chem. Sci.* **2021**, *12*, 911–916.
- [28] Z. Dezhahang, M. Poopari, J. Cheramy, Y. Xu, *Inorg. Chem.* **2015**, *54*, 4539–4549.
- [29] a) M. Losada, Y. Xu, *Phys. Chem. Chem. Phys.* **2007**, *9*, 3127–3135; b) A. S. Perera, J. Thomas, M. R. Poopari, Y. Xu, *Front. in Chem.* **2016**, *4*, 9 (1–17); c) A. S. Perera, J. Cheramy, C. Merten, J. Thomas, Y. Xu, *ChemPhysChem* **2018**, *19*, 2234–2242.
- [30] J. Šebestík, F. Teplý, I. Cisařová, J. Vávra, D. Koval, P. Bouř, *Chem. Commun.* **2016**, *52*, 6257–6260.
- [31] S. O. Pour, L. Rocks, K. Faulds, D. Graham, V. Parchaňský, P. Bouř, E. W. Blanch, *Nat. Chem.* **2015**, *7*, 591–596.
- [32] a) S. Yamamoto, P. Bouř, *J. Comput. Chem.* **2013**, *34*, 2152–2158; b) V. Novák, M. Dendisová, P. Matějka, P. Bouř, *J. Phys. Chem. C* **2016**, *120*, 18275–18280; c) V. Novák, J. Šebestík, P. Bouř, *J. Chem. Theory Comput.* **2012**, *8*, 1714–1720.
- [33] G. Li, J. Kessler, J. Cheramy, T. Wu, M. R. Poopari, P. Bouř, Y. Xu, *Angew. Chem. Int. Ed.* **2019**, *58*, 16495–16498; *Angew. Chem.* **2019**, *131*, 16647–16650.
- [34] G. Placzek, in *Rayleigh and Raman Scattering*, UCRL Trans. No. 526 L from Handbuch der Radiologie (ed. by E. Marx), Leipzig, Akademische Verlagsgesellschaft V1 2, 209, **1934**.
- [35] a) J. Nestor, T. G. Spiro, *J. Raman Spectrosc.* **1973**, *1*, 539–550; b) R. Clark, S. R. Jeyes, A. J. McCaffery, R. A. Shatwell, *J. Am. Chem. Soc.* **1974**, *96*, 5586–5588.
- [36] W. Hug, G. Zuber, A. de Meijere, A. F. Khlebnikov, H.-J. Hansen, *Helv. Chim. Acta* **2001**, *84*, 1–21.
- [37] M. J. Frisch, Gaussian 16, Revision C.01, Gaussian, Inc., Wallingford, CT, **2016**. See Supporting Information for the full reference.
- [38] a) L. Jensen, J. Autschbach, M. Krykunov, G. C. Schatz, *J. Chem. Phys.* **2007**, *127*, 134101; b) L. A. Nafie, *Theor. Chem. Acc.* **2008**, *119*, 39–55; c) T. Helgaker, S. Coriani, P. Jørgensen, K. Kristensen, J. Olsen, K. Ruud, *Chem. Rev.* **2012**, *112*, 543–631.
- [39] M. J. Frisch, Gaussian development version, Gaussian, Inc., Wallingford, CT, **2020**. See Supporting Information for the full reference.
- [40] P. Zardi, K. Wurst, G. Licini, C. Zonta, *J. Am. Chem. Soc.* **2017**, *139*, 15616–15619.
- [41] J. Kapitán, L. D. Barrona, L. Hecht, *J. Raman Spectrosc.* **2015**, *46*, 392–399.

Manuscript received: December 2, 2021

Accepted manuscript online: January 14, 2022

Version of record online: February 14, 2022